DOI: 10.1002/ejic.200901037

Volatile, Monomeric, and Fluorine-Free Precursors for the Metal Organic Chemical Vapor Deposition of Zinc Oxide

Daniela Bekermann,[a] Detlef Rogalla,[b] Hans-Werner Becker,[b] Manuela Winter,[a] Roland A. Fischer,[a] and Anjana Devi*[a]

Keywords: Zinc oxide / Ketoiminato ligands / Chemical vapor deposition / Thin films

Two new bis(ketoiminato)zinc(II) compounds that show excellent precursor properties for the chemical vapor deposition (CVD) of zinc oxide materials are presented. The synthesis of the ketoiminato zinc complexes [Zn{[$(CH_2)_x$-OCH_3]NC(CH_3)=C(H)C(CH_3)=O}$_2$] (**1**: x = 2; **2**: x = 3) is straightforward and can easily be scaled up. Compounds **1** and **2** were analyzed by ^{1}H and ^{13}C NMR spectroscopy, elemental analysis, single-crystal X-ray diffraction analysis, and electron ionization mass spectrometry. The compounds exist as monomers with a distorted tetrahedral zinc center. Thermogravimetric studies, sublimation, and solubility tests reveal very promising properties for metal–organic CVD related applications. Preliminary metal–organic CVD experiments with the use of compound **1** were performed as a screening for the suitability of the new bis(ketoiminato)zinc complexes as precursors for the growth of ZnO thin films in the presence of oxygen. The films were characterized by X-ray diffraction, scanning electron microscopy, energy dispersive analysis of X-ray, and Rutherford backscattering measurements. The as-deposited ZnO films were stoichiometric; the crystalline films exhibited strong preferred orientation along the *c*-axis.

Introduction

Zinc oxide offers various superior features, including optical[1] and piezoelectrical properties,[2,1c] a direct, large band gap of 3.7 eV,[3,1c] a large exciton binding energy of 60 meV, and chemical, thermal, and high radiation stability. Due to its numerous interesting material properties, zinc oxide is a widely used semiconductor oxide and a subject of current research as an advanced functional material for several applications, which include batteries, fuel cells, transparent conducting oxides (TCOs), ferrites, gas sensing,[4] and photovoltaic cells.[5]

Metal–organic chemical vapor deposition (MOCVD) is a preferred technique[1f] for the growth of high-quality materials that can also be adapted to large-scale production. In addition, MOCVD enables conformal step coverage over complex topographies and nanostructured growth. The employed metal–organic precursor plays a key role during the deposition process, as its decomposition directly leads to the formation of the desired material. The commonly used zinc precursor for ZnO is diethylzinc (DEZ)[6] in combination with an oxygen source. Due to the pyrophoric nature of the compound, alternative precursors such as zinc acetate[7a,7e] and zinc acetylacetonate [Zn(acac)$_2$][7b] have been adopted to avoid the handling problems associated with alkylzinc reagents. There have been attempts to develop other suitable precursors, which include [Zn(hfac)$_2$(TMEDA)],[8a] [Zn(tmp)$_2$],[8b] [Zn(TTA)$_2$TMEDA],[8c] [(CH_3)Zn-{OC(CH_3)$_3$}]$_4$,[8d] [EtZnNEt$_2$],[8e] etc.). However, the thermal properties such as high vaporization temperatures and high melting points (136–138 °C) are not so favorable. Therefore, efforts have been made to develop alternatives or improved precursors for ZnO film growth. Recently, two ketoiminato compounds [Zn{(R)NC(CH_3)=C(H)C(R′)=O}$_2$] (R = *n*Bu, R′ = Me; R = *i*Pr, R′ = OEt) were reported that showed one-step-decomposition behavior in thermal gravimetric studies and reasonable melting and evaporation temperatures. However, quite significant carbon incorporation was observed in atmospheric pressure (AP)CVD of ZnO using these precursors.[9]

In the past, we have used the strategy of using chelating ligands, which was shown to work well for the use of malonato-based transition-metal complexes for the formation of the corresponding transition-metal oxides.[10] A similar approach involving the use of bidentate ligands with a goal to obtain monomeric complexes was adopted for Zn.[11] In this study, nitrogen-containing chelating ligands were used, as nitrogen is a weaker donor than oxygen, and thus volatilization and evaporation are expected to occur at lower temperatures than for all oxygen-coordinated complexes like, for example, zinc acetylacetonate. Our efforts were also concentrated on synthesizing halogen-free precursors, and in

[a] Inorganic Materials Chemistry, Lehrstuhl für Anorganische Chemie II, Ruhr-Universität Bochum,
44780 Bochum, Germany
Fax: +49-234-32-14174
E-mail: anjana.devi@rub.de
[b] Dynamitron-Tandem-Laboratorium (DTL) of RUBION, Ruhr-Universität Bochum,
44780 Bochum, Germany
Supporting information for this article is available on the WWW under http://dx.doi.org/10.1002/ejic.200901037.

WILEY InterScience DISCOVER SOMETHING GREAT
© 2010 Wiley-VCH Verlag GmbH & Co. KGaA, Weinheim

this process we developed two new zinc complexes by using ketoiminates as chelating ligands. The zinc bis(ketoiminates) that are presented here are of the type $[Zn\{[(CH_2)_x\text{-}OCH_3]NC(CH_3)=C(H)C(CH_3)=O\}_2]$ (**1**: $x = 2$; **2**: $x = 3$). These newly synthesized compounds exhibit some distinct advantages for them to be applicable for the MOCVD of ZnO. In this paper we discuss the synthesis and characterization of these complexes, and the thermal properties, which are very important for CVD applications, are also evaluated. In addition, the preliminary results on the MOCVD growth and characterization of ZnO thin films with the use of compound **1** are also presented and discussed.

Results and Discussion

Synthesis and Properties of the Precursor

The zinc ketoiminates were obtained by the stoichiometric reaction of DEZ with the neutral ketoiminate in hexane (Scheme 1). As both the compounds are very similar (with a small change in the ligand skeleton), the synthesis procedure, structural, and precursor properties of $[Zn\{[(CH_2CH_2OCH_3)N]C(CH_3)=C(H)C(CH_3)=O\}_2]$ (**1**) will be discussed in detail as a representative example. Compounds **1** and **2** were synthesized in spectroscopically pure form and were identified by ^1H NMR spectroscopy. For compound **1**, the two singlets at $\delta = 1.60$ and 2.00 ppm correspond to the methyl groups attached to the chelate ring, whereas those shifted low field to $\delta = 3.05$ ppm can be attributed to the methyl group of the ether arm. The singlet at $\delta = 4.78$ ppm corresponding to one proton can be attributed to the hydrogen atom at the chelate ring. At $\delta = 3.25$ and 3.46 ppm two broad signals appear with an integration corresponding to four protons; these signals are assigned to the ether side chain.

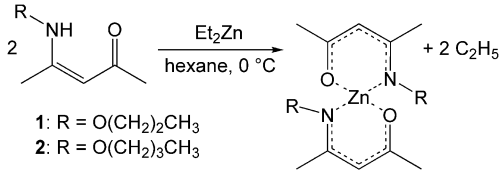

Scheme 1. Reaction scheme for the synthesis of **1** and **2**.

Single-Crystal X-ray Diffraction

Single crystals of **1** suitable for X-ray structural analysis were obtained from a saturated solution of the compound in toluene at –30 °C over a period of 24 h. Molecule **1** crystallizes in the orthorhombic space group $Pca2_1$. The solid-state structure of **1** with an atom-numbering scheme is shown in Figure 1 (Table 4). Molecule **1** is a monomer and it consists of a distorted tetrahedral Zn center with two bidentate ketoiminate ligands. The coordination environment around the zinc is completed by the oxygen and nitrogen atoms of two ketoiminato ligands. These two ketoiminato ligands are orthogonal to each other. The six-membered $ZnONC_3$ units are puckered. The oxygen atoms (O3 and O4) of Me–O–CH_2–CH_2–N are far away from the coordination sphere of the zinc center. The Zn–O bond lengths (Zn1–O1 1.955 Å and Zn1–O2 1.939 Å) in **1** are not equal. Similarly, the Zn1–N2 (1.990 Å) distance is slightly longer than that of Zn1–N1 (1.984 Å). The Zn–O (av. 1.947 Å) bond lengths in **1** are slightly longer than the Zn–O distances found in $[Zn(C_{17}H_{14}ClN_2O)_2]$ [1.907(1) Å], whereas the Zn–N (av. 1.992 Å) distances are shorter than the Zn–N distances of $[Zn(C_{17}H_{14}ClN_2O)_2]$ [2.016(1) Å].[12] The ketoiminato ligands are not equal in symmetry, which was also predicted by DFT calculations (Table S4, Supporting Information). In addition, the crystal structure indicates that the electrons are not completely delocalized in the six-membered ring. The facts leading to this assumption are described below: (i) The bite angles of the chelating ligands are 97.3 and 97.1°, respectively, and the angles O2–Zn1–N1, O1–Zn1–N2, O1–Zn1–O2, and N1–Zn1–N2 vary between 108.53(5) and 125.41(6)°, deviating from those expected for an ideal tetrahedron. (ii) As expected, the Zn–O bonds with lengths of 1.955(1) and 1.939(1) Å are longer than those for the Zn–N bonds [1.990(2) Å and 1.984(2) Å]. (iii) The torsion angles indicate a nonplanar six-membered ring (see Table S3, Supporting Information). A system containing completely delocalized π-electrons is expected to be planar due to the sp^2-hybridized carbon atoms. Indeed, the torsion angles of O1, C1, C7, C2, C3, C8, N1, and C9 vary between ca. 2 and 5°. The torsion angles between the above-mentioned atoms of the sixfold ring and the zinc center are even around 10° (the same is observed for the torsion angles of the second chelate ligand).

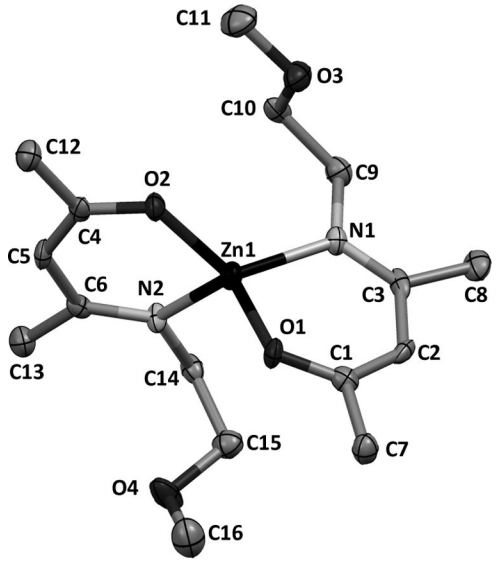

Figure 1. Molecular structure of **1**. Hydrogen atoms are removed for clarity. Selected bond lengths [Å] and angles [°]: Zn1–O2 1.939(1), Zn1–O1 1.955(1), Zn1–N1 1.984(2), Zn1–N2 1.990(2), O1–C1 1.288(2) and O2–Zn1–O1 108.53(5), O2–Zn1–N1 125.41(6), O1–Zn1–N1 97.29(6), O2–Zn1–N2 97.14(6), O1–Zn1–N2 116.19(6), N1–Zn1–N2 113.46(6).

 © 2010 Wiley-VCH Verlag GmbH & Co. KGaA, Weinheim

Density Functional Theory (DFT) Calculations

DFT calculations were carried out in order to estimate the thermodynamic stability of the molecules. The Gibbs free energies of formation $\Delta_r G^0$(298 K) were calculated on the basis of the following reaction:

$\{(CH_2CH_2OCH_3)N(H)C(CH_3)=C(H)_2C(CH_3)=O\} + [Zn(CH_2CH_3)_2] \rightarrow Zn\{[(CH_2CH_2OCH_3)N]C(CH_3)=C(H)C(CH_3)=O\}_2 + CH_3CH_3$

The values of the Gibbs free energies of reaction of formation of **1** and **2** are highly negative, clearly indicating a thermodynamically favored reaction pathway. There are only minor differences in the calculated Gibbs energies of **1** and **2**, pointing to similar stabilities of these compounds. The calculations on **1** and **2** gave a Gibbs free energy of $\Delta_r G^0$(298 K) = –81 and –78 kcal mol^{-1}, respectively. The molecular structure of **1** obtained by DFT calculation was compared with that derived from single-crystal X-ray diffraction measurements to evaluate the performance of the theoretical results. The data were in good agreement with each other (Table S4, Supporting Information). Thus, the results obtained by this theoretical method should be reliable.

Mass Spectrometry

The fragmentation mechanism of bis(ketoiminato) precursors **1** and **2** was examined by electron impact ionization mass spectrometry (EI-MS). However, care must be taken to extrapolate the fragmentation data to the thermal conditions of the MOCVD experiment. All recorded mass spectra (Table S5, Supporting Information) strongly support the complete cleavage of the whole ligand under EI-MS conditions (Table 1).

Thermal Properties and Solubility

The melting points of **1** and **2** are 57 and 60 °C, respectively. These values are advantageous and quite low compared to the most commonly used precursor for ZnO, namely, [Zn(acac)$_2$] (136–138 °C)[13] (Table 2). Both **1** and **2** can be quantitatively and repeatedly vaporized at 110 and 115 °C, respectively, at 5 mbar, without any decomposition. As revealed by thermal analysis, the compounds are volatile and the thermogravimetric analysis (Figure 2) shows a nearly one-step decomposition for both compounds, which is desirable for MOCVD precursors. The temperature window between vaporization and decomposition is sufficiently large. The temperature onset of volatilization (≈1 % mass loss) in the case of **1** is 70 °C, whereas in the case of **2** it is 90 °C. For **1**, a strong mass loss occurs between 130 and 280 °C, whereas the main mass loss for compound **2** start around 150 °C. This shows that a marginal variation in the ligand structure has a distinct influence on the volatilization temperature.

Table 2. Melting points of ZnO precursors.

Compound	M.p. [°C]	Ref.
1	57	
2	60	
[Zn{(*n*Bu)NC(CH$_3$)=C(H)C(Me)=O}$_2$]	72	[9]
[Zn{(*i*Pr)NC(CH$_3$)=C(H)C(OEt)=O}$_2$]	109	[9]
[Zn(acac)$_2$]	136–138	[7]
[Zn(tta)$_2$tmeda]		[8c]

(Htta = 2-theonyltrifluoroacetone, tmeda = tetramethylethylene diamine)

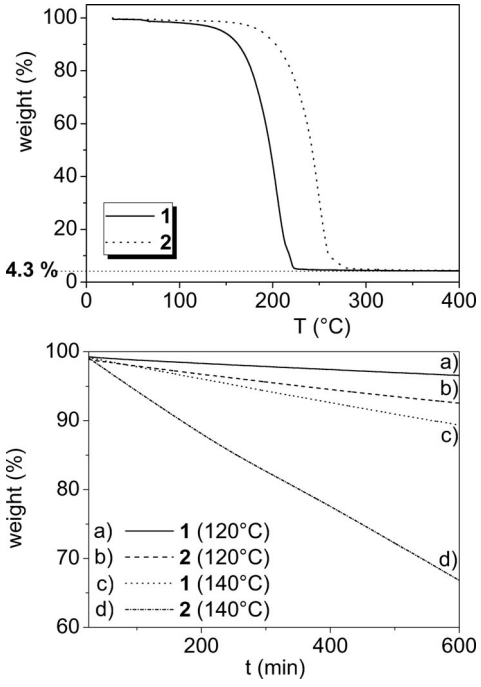

Figure 2. Thermal analysis of **1** and **2**. Top: Thermal gravimetric analysis (TGA) (5 K min^{-1}, 300 mL min^{-1}); bottom: isothermal vaporization studies of **1** and **2** at different temperatures.

Table 1. EI-MS data for **1** and **2**.

Compound **1** Fragments	Mass [*m*/*z*]	Relative intensity [%]	Compound **2** Fragments	Mass [*m*/*z*]	Relative intensity [%]
$M^{+\cdot}$	376	2.0	$M^{+\cdot}$	404	13.8
$M^{+\cdot} - Me^{\cdot}$	361	1.6	$M^{+\cdot} - Me^{\cdot}$	389	2.0
$M^{+\cdot} - OCH_3^{\cdot}$	345	9.8	$M^{+\cdot} - OCH_3^{\cdot}$	373	0.3
$361 - C_2H_6$ or $- CH_2O^{\cdot}$	331	13.8	$M^{+\cdot} - C_3H_5^{\cdot}$	363	1.0
or $M^{+\cdot} - CH_2OCH_3^{\cdot}$			$M^{+\cdot} - 58^{\cdot}$	346	1.0
$M^{+\cdot}$ – 1 ligand	220	100	$M^{+\cdot}$ – 1 ligand	234	100
			$OC_3H_6^{\cdot}$ or NC_3H_8	58	

 © 2010 Wiley-VCH Verlag GmbH & Co. KGaA, Weinheim

The thermal stability and sublimation behavior of the ketoiminato precursors was further investigated by isothermal TG experiments carried out at 120 and 140 °C. In all cases, linear weight loss was observed (Figure 2), indicating that the precursor can sublime at the set temperature with constant rates for a long period of time. The sublimation rates at 120 °C were determined to be 9.3 $\mu g\,min^{-1}$ for **1** and 20.1 $\mu g\,min^{-1}$ for **2**. The linear trends in the isothermal curves show clean vaporization processes with no signs of premature decomposition. Another desirable feature is that both **1** and **2** are readily soluble in a wide range of common organic solvents such as hexane, pentane, benzene, toluene, etc. This property makes them suitable also for applications such as liquid injection MOCVD or wet chemical deposition methods.

MOCVD of ZnO with the use of Compound 1

ZnO Film Growth

On the basis of the promising thermal properties, the applicability of this class of complexes as precursors for MOCVD applications was verified by carrying out preliminary deposition by using **1**, which as discussed earlier, showed higher volatility than **2**. ZnO thin films were grown on Si(100) substrates in the temperature range 450–700 °C (film1–film5; Figures 3 and 4 and Table 3) by using oxygen as the reactive gas. The films were very uniform, adherent to the substrate (scotch-tape test), and shiny in appearance. The dependence of film growth rate as a function of substrate temperature is depicted in Figure 3. The film thickness was determined from cross-section SEM measurements and the growth rates (GR) were thereby derived. From the Arrhenius plot (Figure 3) it can be seen that there is a gradual increase in GR in the temperature range 450–600 °C (kinetically controlled region) with GRs of the order of 4.2–20.5 $Å\,min^{-1}$. Between 600 and 650 °C there is not much variation in the GR. Beyond 650 °C, there is a steady decline in the GR, which could be due to precursor depletion or gas-phase reactions that are likely to occur at higher temperatures. More detailed studies varying different CVD process parameters are warranted to confirm this.

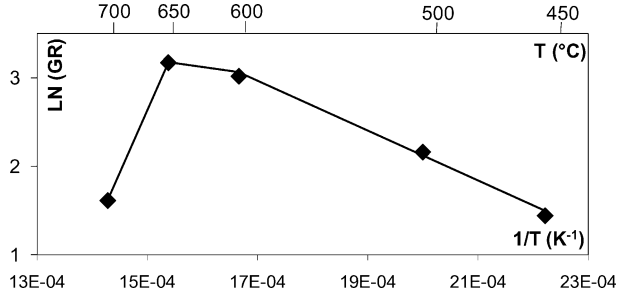

Figure 3. Arrhenius plot of the growth rate (GR) of ZnO as a function of substrate temperature ($1/T$) with the use of compound **1**.

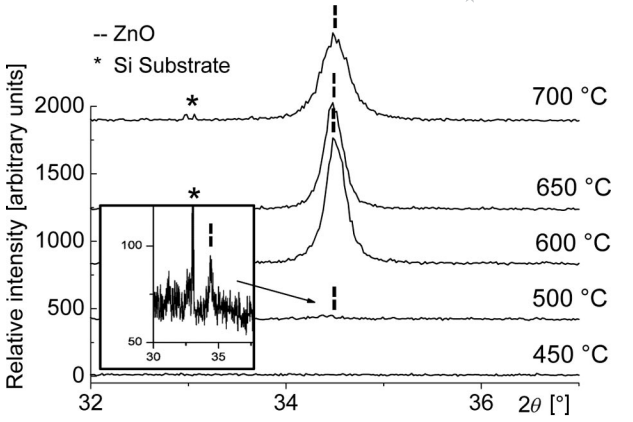

Figure 4. XRD pattern of ZnO deposited on Si(100) substrates by using compound **1** (see also Figure S1, Supporting Information).

Table 3. Process conditions for the deposition of ZnO on Si(100) at a reactor pressure of 1 mbar.

Sample name	Substrate temperature [°C]
Film1	450
Film2	500
Film3	600
Film4	650
Film5	700

Film Crystallinity

The onset temperature for film growth was 450 °C (film1), in which case the as-deposited film was amorphous. All depositions performed between 500 and 700 °C (film2–film5) show the growth of the hexagonal ZnO wurtzite structure (PDF 00–036–1451, Zincite phase). In all cases, the only observed pattern at $2\theta = 34.4°$ can be attributed to the (002) reflection of Zincite. The as-deposited zinc oxide structures for substrate temperatures of 500, 600, 650, and 700 °C, respectively, show a strong preferential orientation along the *c*-axis. Evaluation of the preferred orientation was performed by a commonly used method.[14]

T_{hkl} is the texture coefficient of a reflex corresponding to (hkl); $I_m(hkl)$ is the related intensity of the measured Bragg reflex and $I_0(hkl)$ its intensity in the standard powder spectrum (PDF 00–036–1451). Because the 002 reflex is the only observed reflex, anisotropic growth was found to be 1 for all samples film2–film5 (Table S6, Supporting Information). The raw intensity is highest for film3 deposited at 600 °C (Table S7, Supporting Information).

Surface Morphology

The surface morphology of the ZnO layers was investigated and some representative SEM plane view and cross-section images are shown in Figure 5. The morphology follows the same trend in terms of temperature dependency as already observed for the growth rates and XRD data: The thickness and crystallinity of the as-deposited ZnO thin films increases from 450 to 600 °C. At 450 °C, (film1) nearly

 © 2010 Wiley-VCH Verlag GmbH & Co. KGaA, Weinheim

featureless material of 40 nm in thickness was grown. At 500 °C, (film2) the thickness of the deposit is 75 nm and a columnar-like densely packed film is seen in the SEM images. In the cross-sectional SEM image (Figure S2, Supporting Information), the columnar structure normal to the substrate indicates a *c*-axis orientation of the films, which is in agreement with results observed in XRD measurements. The ZnO thin film deposited at 600 °C (film3) exhibits the highest thickness (210 nm), which is in agreement with the observation made by XRD. The XRD 002 pattern of film3 has the highest raw intensity among all ZnO deposits. The ZnO material grown at higher temperatures (film4 and film5) have very similar morphologies (Figure 5) to that of film3, but their film thicknesses are lower (175 and 45 nm). Also, the raw intensities of the corresponding XRD 002 patterns are lower for film4 and film5 than for film3.

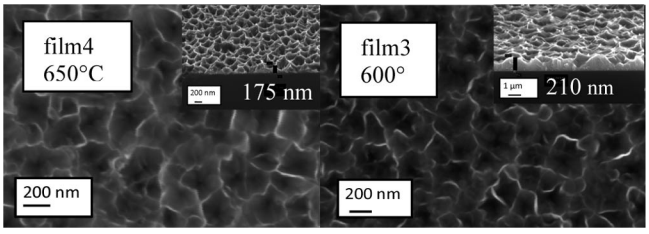

Figure 5. Cross-section and plane view SEM images of film3 and film4.

Film Composition

The film composition was analyzed by EDX and revealed the presence of zinc and oxygen (Figure S3, Supporting Information). Carbon could not be detected. However, EDX is not a sensitive method to detect lighter elements like carbon. Rutherford backscattering (RBS) was employed to determine the film stoichiometry, and the presence of Zn and O in the spectra of a ZnO film grown at 600 °C is clearly seen (Figure 6). The thickness of the layer is in agreement with the value determined by the SEM image (Figure 5), taking into account the surface roughness. The recorded spectrum is described by a simulation of a 190-nm thick layer of zinc (41 at.-%), oxygen (45 at.-%) deposited on a silicon substrate. In comparison to the data with the simulation, the broadening of the Si edge and of the low-energy Zn edge can be attributed to the surface roughness of the layer (Figure 5). The spectrum indicates the presence of carbon in the range of 5 wt.-%, thus indicating that the precursor is able to provide the ZnO material in the right stoichiometry. Further characterization techniques like XPS/AES (depth profile) are warranted for precise quantification of residual trace impurities that may be present in the bulk of the films, especially for lighter elements such as carbon and nitrogen. These measurements as well as the investigation of optical properties by UV/Vis and photoluminescence spectroscopy (PL) are currently underway.

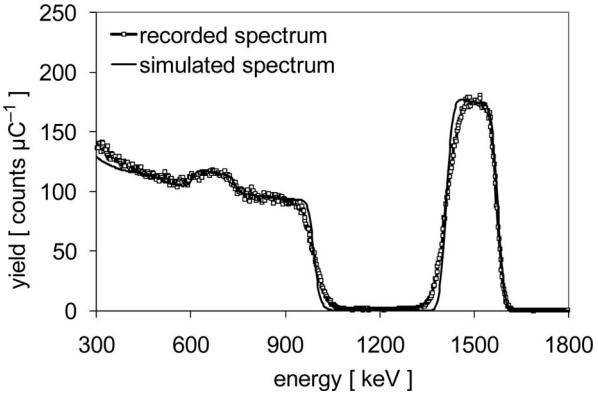

Figure 6. Representative RBS spectrum of ZnO grown at 600 °C by using compound **1**.

Conclusions

Two new zinc complexes with ketoiminates as chelating ligands were synthesized and characterized. The synthesis procedure is simple and very straightforward, and the products can be isolated in good yields and easily scaled up. The crystal structure of **1** was determined, and the complex reveals a four-coordinated zinc metal center that exhibits a distorted tetrahedral ligand environment. The above-highlighted zinc complexes are relatively stable towards humidity, can be easily handled, and are very soluble and stable in common organic solvents. The thermal properties are very encouraging in terms of low melting points, good volatility, and clean decomposition characteristics. The suitability of this class of complexes for MOCVD is demonstrated by successfully growing stoichiometric and oriented ZnO thin films. The film morphology was strongly dependent on substrate temperature and very rough crystalline ZnO was obtained at 600–700 °C. A high surface area is desirable for potential applications such as gas sensors or photo cells, which will be the focus of our research work in the near future. The data presented reveals the potential of the zinc ketoiminate compounds as improved precursors for ZnO-based materials.

Experimental Section

General: All manipulations of air- and moisture-sensitive compounds were performed in a conventional vacuum/argon line by using standard Schlenk techniques. Pure DEZ was purchased from ABCR and used as received. Preparations of samples for further analysis were carried out in argon-filled glove boxes (MBraun, LabMaster). All solvents were purified by an MBraun solvent purification system (SPS) and stored over molecular sieves (4 Å). NMR solvents were degassed and dried with activated molecular sieves. Elemental analysis was performed by the Analytical Service Centre of the Chemistry Department (CHNSO Vario EL 1998). The ^{1}H and ^{13}C NMR spectra were recorded with a Bruker Advance DPX-250 instrument and referenced to internal solvents (residual proton signals) and corrected to the TMS (tetramethylsilane) standard values. For the COSY and HMBC NMR spectra, a Bruker-DRX-400 and a Bruker-DRX-600 instrument were used. Single-crystal diffraction experiments were carried out at 112 K with an Oxford

 © 2010 Wiley-VCH Verlag GmbH & Co. KGaA, Weinheim

Xcalibur 2 CCD/PD diffractometer with monochromated Mo-K_α radiation (0.71073 Å). The structure was solved by direct methods and refined anisotropically with the SHELXL-97 program suite.[15] Refinement details for **1** are summarized in Table 4. CCDC-752098 (for **1**) contains the supplementary crystallographic data for this paper. These data can be obtained free of charge from The Cambridge Crystallographic Data Centre via www.ccdc.cam.ac.uk/data_request/cif. Electron ionization mass spectra (EI-MS) were recorded at 70 eV by using a Varian MAT spectrometer. Simultaneous thermogravimetric and differential thermal analysis (TG/DTA) was carried out by using a Seiko TG/DTA 6300S11 at ambient pressure (Sample size ≈10 mg), with a heating rate of 5 °C min^{-1} (N_2 flow rate = 300 mL min^{-1}). For the DFT studies, Gaussian 03[16] was used. B3LYP was used as a hybrid functional with double zeta base and a LANL2 potential. The software program Molden[17] was used to calculate the bond lengths and angles of the molecular structures. The final image was displayed by use of the freeware program Mercury (Hg) from CCDC. The calculations do not take into account the solvent effects.

Table 4. Crystal data and structure refinement for $C_{16}H_{28}N_2O_4Zn$ (**1**) at 112 K.

	$C_{16}H_{28}N_2O_4Zn$
Formula weight	377.80
Crystal system, space group	orthorhombic, $Pca2_1$
a [Å]	21.7459(6)
b [Å]	5.66530(10)
c [Å]	14.5000(3)
α [°]	90
β [°]	90
γ [°]	90
Volume [Å^3]	1786.36(7)
Z	4
Calculated density [g cm^{-3}]	1.405
Absorption coefficient [mm^{-1}]	1.395
F(000)	800
Reflections collected/unique	13135/3119 [R(int) = 0.0224]
Observed reflns[$I > 2\sigma(I)$]	2789 $F_o > 4\sigma(F_o)$
Goodness-of-fit on F^2	0.965
Final R indices [$I > 2\sigma(I)$]	R_1 = 0.0182, wR_2 = 0.0411
Absolute structure parameter	–0.007(9)
Largest difference in peak and hole [e Å^{-3}]	0.208 and –0.166

MOCVD screening experiments were carried out by using a self-built horizontal MOCVD cold-wall reactor as described elsewhere.[18] The substrates used were Si (100)-wafers (≈1.4 × 2.0 cm). The wafers were cleaned in an ultrasonic bath of ethanol for 10 min and in an ultrasonic bath of pure water for 10 min and then dried. The reactor pressure was kept constant at 10 mbar for all depositions. Nitrogen 6.0 was used as carrier gas and oxygen as reactive gas. The flow rates of nitrogen and oxygen were maintained at 50 sccm for all depositions. ZnO was grown at different temperatures between 450 and 700 °C (film1–film5) by using an inductive high frequency heating system. A bubbler temperature of 120 °C was used for precursor evaporation. The deposition time was set to 90 min for all MOCVD experiments. Film thickness and corresponding growth rates were estimated from cross-sectional SEM data. Thin-film X-ray diffraction (XRD) measurements were performed by using a Bruker AXS D8 Advance diffractometer with Cu-K_α radiation (1.5418 Å). The surface morphology of the films was determined by scanning electron microscopy (SEM) by using a LEO 1530 Gemini instrument (Zeiss). The composition of the films was determined by EDX and RBS. The RBS measurements have been performed at the Dynamitron-Tandem-Laboratory at the University of Bochum by using a singly charged He beam with the energy of 2 MeV and a beam current of 20–40 nA. A silicon surface barrier detector was placed at an angle of 160° with respect to the beam axis. The solid angle of the detector was 1.911 msrad. The spectra were analyzed with the program RBX.

[Zn{[(CH$_3$OCH$_2$CH$_2$)*N*]C(CH$_3$)=C(H)C(CH$_3$)=*O*}$_2$] (1): Diethylzinc (DEZ) (3 mL, 29.39 mmol) was dissolved in dry hexane (150 mL). The solution was stirred for 12 h and cooled down to –15 °C. To this mixture was added {(CH$_3$OCH$_2$CH$_2$)NH-[C(CH$_3$)=C(H)C(CH$_3$)=O]} (7.11 mL, 58.78 mmol) by syringe. The reaction was heated at reflux for 1.5 h and afterwards stirred for 12 h at room temperature. The solvent was removed in vacuo at room temperature. The solid residue was washed with dry pentane (3 × 5 mL) and dried again. The product was obtained as a light-yellow powder (8.81 g, 23.43 mmol, 79.7%). M.p. 56–57 °C. $C_{16}H_{28}N_2O_4Zn$ (377.80): calcd. C 51.07, H 7.45, N 7.45; found C 51.02, H 7.48, N 7.48. ^{1}H NMR (250 MH*z*, C_6D_6, 25 °C): δ = 1.57 [s, 6 H, -NC(C*H*$_3$)], 1.97 [s, 6 H, -OC(C*H*$_3$)], 3.05 [s, 6 H, N(CH$_2$)$_2$-OC*H*$_3$], 3.25 and 3.46 [2 m, 8 H, -N(C*H*$_2$)$_3$CH$_3$], 4.80 [s, 2 H, OC(CH$_3$)C(*H*)C(CH$_3$)N] ppm. ^{13}C NMR (100.6 MHz, C_6D_6, 25 °C): δ = 22.02 [NC(*C*H$_3$)], 27.84 [OC(*C*H$_3$)], 50.51 [N(*C*H$_2$)$_2$-O(CH$_3$)], 58.45 [N(CH$_2$)$_2$O(*C*H$_3$)], 96.87 [OC(CH$_3$)*C*(H)C(CH$_3$)-N], 172.48 [OC(CH$_3$)C(H)*C*(CH$_3$)N], 183.47 [O*C*(CH$_3$)C(H)C-(CH$_3$)N] ppm. EI-MS (70eV): *m*/*z* (%) = 376 (2.0) [M$^{+\cdot}$], 361 (1.6) [M$^{+\cdot}$ – CH$_3$], 345 (9.8) [M$^{+\cdot}$ – OCH$_3^{\cdot}$], 331 (13.8) [M$^{+\cdot}$ – OCH$_3^{\cdot}$], 220 (100) [M$^{+\cdot}$ – 1 ligand].

[Zn{[(CH$_3$OCH$_2$CH$_2$CH$_2$)*N*]C(CH$_3$)=C(H)C(CH$_3$)=*O*}$_2$] (2): The synthesis procedure was similar to that adopted for **1**. DEZ (3 mL, 29.39 mmol) was treated with {(CH$_3$OCH$_2$CH$_2$CH$_2$)NH-[C(CH$_3$)=C(H)C(CH$_3$)=O]} (7.68 mL, 58.78 mmol). The product was obtained as a light-yellow powder (8.00 g, 19.80 mmol, 67.3%). M.p. 59–60 °C. $C_{18}H_{32}N_2O_4Zn$ (405.85): calcd. C 53.47, H 7.92, N 6.93; found C 53.51, H 7.93, N 6.86. ^{1}H NMR (250 MH*z*, C_6D_6, 25 °C): δ = 1.61 [s, 6 H, -NC(C*H*$_3$)], 1.86 (quint., $^3J_{H,H}$ = 6.63 Hz, 4 H, NCH$_2$C*H*$_2$CH$_2$OCH$_3$), 2.01 [s, 6 H, -OC(C*H*$_3$)], 3.02 [s, 6 H, N(CH$_2$)$_3$OC*H*$_3$], 3.16 (t, $^3J_{H,H}$ = 5.84 Hz, 4 H, NCH$_2$CH$_2$-C*H*$_2$OCH$_3$), 3.32 (t, $^3J_{H,H}$ = 6.48 Hz, 4 H, NC*H*$_2$CH$_2$CH$_2$OCH$_3$), 4.80 [s, 2 H, OC(CH$_3$)C(*H*)C(CH$_3$)N] ppm. ^{13}C NMR (100.6 MHz, C_6D_6, 25 °C): δ = 21.40 [NC(*C*H$_3$)], 27.77 [OC(*C*H$_3$)], 31.36 (NCH$_2$*C*H$_2$CH$_2$OCH$_3$), 48.06 (NCH$_2$CH$_2$*C*H$_2$OCH$_3$), 58.15 [N(CH$_2$)$_2$O(*C*H$_3$)], 70.17 (N*C*H$_2$CH$_2$CH$_2$OCH$_3$), 96.87 [OC(CH$_3$)-*C*(H)C(CH$_3$)N], 172.48 [OC(CH$_3$)C(H)*C*(CH$_3$)N], 183.47 [O*C*-(CH$_3$)C(H)C(CH$_3$)N] ppm. EI-MS (70eV): *m*/*z* (%) = 404 (14) [M$^{+\cdot}$], 389 (2) [M$^{+\cdot}$ – CH$_3^{\cdot}$], 372 (0.3) [M$^{+\cdot}$ – OCH$_3^{\cdot}$], 234 (100) [M$^{+\cdot}$ – 1 ligand].

Supporting Information (see footnote on the first page of this article): Additional crystal data for **1** regarding structure refinement, bond lengths, angles, torsion angles, and comparison with the crystal structure derived from DFT calculation;. detailed EI-MS data, further XRD data including raw intensities and texture coefficients of ZnO1–ZnO5, and full 2θ-range spectrum; figure showing a cross-section SEM image of film2, and a representative EDX spectrum for an as-grown ZnO film deposited on Si(100) by using compound **1**.

Acknowledgments

The authors thank Andrian Milanov for synthesizing and providing the ketoiminato ligands that were used for the syntheses of **1** and **2**. D. B. is grateful to the integrated Graduate College of the Research Centre in Metal Support Interaction in Heterogeneous

 © 2010 Wiley-VCH Verlag GmbH & Co. KGaA, Weinheim

Catalysis at the Ruhr University Bochum for the award of a fellowship.

[1] a) M. Wu, T. Shiosaki, A. Kawabata, *IEEE J. Quantum Electron.* **1989**, *25*, 252–256; b) M. Wu, T. Shiosaki, A. Kawabata, *IEEE J. Quantum Electron.* **1987**, *23*, 1105–1107; c) H. Morkoc, Ü. Özgür, *Zinc Oxide – Fundamentals, Materials and Device Technology*, 1st ed., Wiley-VCH, Berlin, **2009**, p. 477; d) C. Periasamy, P. Chakrabarti, *J. Vac. Sci. Technol. B* **2009**, *27*, 2124–2127; e) D. J. Gargas, M. E. Toimil-Molares, Pl. Yang, *J. Am. Chem. Soc.* **2009**, *131*, 2125–2127; f) W. I. Park, *Met. Mater. Int.* **2008**, *14*, 659–665.

[2] a) Z. L. Wang, J. H. Song, *Science* **2006**, *312*, 242–246; b) M. Alexe, S. Senz, M. A. Schubert, D. Hesse, U. Gösele, *Adv. Mater.* **2008**, *20*, 4021–4026.

[3] Ü. Özgür, Y. I. Alivov, C. Liu, A. Teke, M. A. Reshchikov, S. Dogan, V. Avrutin, S.-J. Cho, H. Morkoc, *J. Appl. Phys.* **2005**, *98*, 041301-1–041301-103.

[4] a) Q. Wan, Q. Li, Y. Chen, T. Wang, X. He, J. Li, C. Lin, *Appl. Phys. Lett.* **2004**, *84*, 3654–3656; b) J. F. Zang, C. M. Li, X. Q. Cui, J. X. Wang, X. W. Sun, H. Dong, *Electroanalysis* **2007**, *19*, 1008–1014; c) G. Sberveglieri, *Sens. Actuators B* **1995**, *23*, 103–109.

[5] a) R. Groenen, J. Loeffler, J. Linden, R. Schropp, M. van de Sanden, *Thin Solid Films* **2005**, *492*, 298–306; b) H. Liu, J. Yang, J. Liang, Y. Huang, C. Tang, *J. Am. Chem. Soc.* **2009**, *91*, 1287–1291; c) Y. Zhang, F. Zhu, J. Zhang, L. Xia, *Nanoscale Res. Lett.* **2008**, *3*, 201–204.

[6] a) J. Hu, R. G. Gordon, *J. Appl. Phys.* **1992**, *71*, 880–890; b) W. Wieldraaijer, J. Van Balen Blanken, E. W. Kuiopers, *J. Cryst. Growth* **1993**, *126*, 305–308; c) I. Alessandri, M. Zucca, M. Ferroni, E. Bontempi, L. E. Depero, *Cryst. Growth Des.* **2009**, *9*, 1258–1259; d) D. C. Kim, J. H. Lee, H. K. Cho, J. H. Kim, J. Y. Lee, *Cryst. Growth Des.* **2009**, *10*, 321–326.

[7] a) S. Jain, T. T. Kodas, M. Hampden-Smith, *Chem. Vap. Deposition* **1998**, *4*, 51–59; b) T. Minami, H. Sato, H. Sonohara, S. Takata, T. Miyata, I. Fukuda, *Thin Solid Films* **1994**, *253*, 14–19; c) K. Kamata, J. Nishino, S. Ohshio, K. Maruyama, M. Ohtuku, *J. Am. Ceram. Soc.* **1994**, *77*, 505–508; d) T. Minami, H. Sonohara, S. Takata, H. Sato, *Jpn. J. Appl. Phys.* **1994**, *33*, L743; e) J.-J. Wu, S.-C. Liu, *J. Phys. Chem. B* **2002**, *106*, 9546–9551.

[8] a) J. Ni, H. Yan, A. Wang, Y. Yang, C. L. Stern, A. W. Metz, S. Jin, L. Wang, T. J. Marks, J. R. Ireland, C. R. Kannewurf, *J. Am. Chem. Soc.* **2005**, *127*, 5613–5624; b) S. Suh, L. A. Mîinea, D. M. Hoffman, Z. Zhang, W.-K. Chu, *J. Mater. Sci. Lett.* **2001**, *20*, 115–118; c) G. Malandrino, M. Blandino, L. M. S. Perdicaro, I. L. Fragala, P. Rossi, P. Dapporto, *Inorg. Chem.* **2005**, *44*, 9684–9689; d) J. Auld, D. J. Houlton, A. C. Jones, S. A. Rushworth, M. A. Malik, P. O'Brien, G. W. Critchlow, *J. Mater. Chem.* **1994**, *4*, 1249–1253; e) S. Suh, D. M. Hoffman, L. M. Atagi, D. C. Smith, *J. Mater. Sci. Lett.* **1999**, *18*, 789–791.

[9] J. S. Matthews, O. O. Onakoya, T. S. Ouattara, R. J. Butcher, *Dalton Trans.* **2006**, 3608–3811.

[10] a) R. Pothiraja, A. Milanov, H. Parala, M. Winter, R. A. Fischer, A. Devi, *Dalton Trans.* **2009**, *4*, 654–663; b) M. Hellwig, K. Xu, D. Barreca, A. Gasparotto, M. Winter, E. Tondello, R. A. Fischer, A. Devi, *Eur. J. Inorg. Chem.* **2009**, 1110–1117.

[11] D. Bekermann, D. Pilard, R. A. Fischer, A. Devi, *ECST* **2009**, *25*, 601–608.

[12] H. M. Ali, M. I. M. Mustafa, M. R. Rizal, S. W. Ng, *Acta Crystallogr., Sect. E* **2008**, *64*, m421.

[13] http://chemicalland21.com.

[14] S. Zhang, D. Sun, Y.-q. Fu, H. Du, Q. Zhang, *J. Metastable Nanocryst. Mater.* **2005**, *23*, 175–178.

[15] G. M. Sheldrick, *SHELXL-97, Program for Refinement of Crystal Structures*, University of Göttingen, Germany, **1997**.

[16] M. J. Frisch, G. W. Trucks, H. B. Schlegel, G. E. Scuseria, M. A. Robb, J. R. Cheeseman, J. A. Montgomery Jr., T. Vreven, K. N. Kudin, J. C. Burant, J. M. Millam, S. S. Iyengar, J. Tomasi, V. Barone, B. Mennucci, M. Cossi, G. Scalmani, N. Rega, G. A. Petersson, H. Nakatsuji, M. Hada, M. Ehara, K. Toyota, R. Fukuda, J. Hasegawa, M. Ishida, T. Nakajima, Y. Honda, O. Kitao, H. Nakai, M. Klene, X. Li, J. E. Knox, H. P. Hratchian, J. B. Cross, V. Bakken, C. Adamo, J. Jaramillo, R. Gomperts, R. E. Stratmann, O. Yazyev, A. J. Austin, R. Cammi, C. Pomelli, J. W. Ochterski, P. Y. Ayala, K. Morokuma, G. A. Voth, P. Salvador, J. J. Dannenberg, V. G. Zakrzewski, S. Dapprich, A. D. Daniels, M. C. Strain, O. Farkas, D. K. Malick, A. D. Rabuck, K. Raghavachari, J. B. Foresman, J. V. Ortiz, Q. Cui, A. G. Baboul, S. Clifford, J. Cioslowski, B. B. Stefanov, G. Liu, A. Liashenko, P. Piskorz, I. Komaromi, R. L. Martin, D. J. Fox, T. Keith, M. A. Al-Laham, C. Y. Peng, A. Nanayakkara, M. Challacombe, P. M. W. Gill, B. Johnson, W. Chen, M. W. Wong, C. Gonzalez, J. A. Pople, *Gaussian 03*, Revision C.02, Gaussian, Inc., Wallingford, CT, **2004**.

[17] G. Schaftenaar, S. Ohapkin, A. da Silva, *Molden*, http://www.cmbi.ru.nl/moldenwindowsnt95.html.

[18] A. Devi, W. Rogge, A. Wohlfart, F. Hipler, H.-W. Becker, R. A. Fischer, *Chem. Vap. Deposition* **2000**, *6*, 245–252.

Received: October 26, 2009
Published Online: February 12, 2010

 © 2010 Wiley-VCH Verlag GmbH & Co. KGaA, Weinheim